Tropical Cyclone-like Vortices in a Limited Area Model: Comparison with Observed Climatology

KEVIN WALSH AND IAN G. WATTERSON

CSIRO Division of Atmospheric Research, Aspendale, Australia

(Manuscript received 8 April 1996, in final form 13 January 1997)

ABSTRACT

A climate simulation of a limited area model implemented over the Australian region is analyzed for the presence of low pressure systems that have some of the physical characteristics of tropical cyclones. The model is run at a horizontal resolution of 125 km and is nested within a GCM simulation of 10 Januarys. The model simulates those variables that are believed to be important for tropical cyclone formation reasonably well, as evaluated using Gray's Seasonal Genesis Parameter. Objective criteria are used to detect tropical cyclone-like vortices (TCLVs) in the model. The composite structure of the simulated storms and the life cycle of a typical TCLV are described. Like tropical cyclones, the simulated TCLVs have warm cores, low-level wind maxima, and their tracks and regions of occurrence are similar to those observed for tropical cyclones. In general, the TCLVs simulated by the limited area model are weaker than observed, as determined by a measure of the area-averaged low-level tangential wind speed, but they are much more realistic than those vortices similarly generated by the GCM. Maximum wind speeds also occur farther from the center of the storm on average than observed. A multiply nested limited area model simulation at a horizontal resolution of 30 km shows further improvement in the TCLV simulation. While the 125-km resolution model may have some potential for predicting genesis regions, numbers, and tracks of TCLVs, it does not yet show such potential for predicting intensities.

1. Introduction

Limited area models (LAMs) have been used to simulate the mean climate of various regions of the globe (Giorgi et al. 1993; Giorgi et al. 1994; McGregor and Walsh 1994; Walsh and McGregor 1995). Less work has been performed on analysis of the variability of such models. In particular, it remains controversial whether climate models running at even a relatively high resolution can simulate some of the characteristics of smaller-scale features such as tropical cyclones. The work of Broccoli and Manabe (1990), Wu and Lau (1992), and Haarsma et al. (1993) used global models of fairly low horizontal resolution (a few hundred kilometers) and analyzed their output to identify systems that had similar structures in some respects to tropical cyclones. An argument against such a strategy is that examination of the typical observed tropical cyclone structure (Frank 1977) suggests that at this resolution intense tropical cyclones may not be reliably differentiated from other less intense tropical low pressure systems. The more recent study of Bengtsson et al. (1995, hereafter B95) was performed at a much higher resolution (T106, roughly equivalent to a grid spacing of 1.125°). At this resolution, observations suggest that there may be some hope of simulating several of the characteristics of tropical cyclones, albeit with a greatly simplified structure compared to reality. Liu et al. (1994) and Hirakuchi and Giorgi (1995) briefly examined the ability of a LAM to generate tropical lows. They found that when the model was driven by the European Centre for Medium-Range Forecasts (ECMWF) analyses, it simulated vortices that were about of the same number and intensity as those represented in the analyses—although the representation of tropical cyclones in the analyses shows some differences from the best available observations (e.g. Walsh 1997). Tsutsui and Kasahara (1996) showed that a T42 resolution GCM could simulate realistic climatological patterns of tropical cyclone formation.

LAMs may be used to obtain even higher resolution more economically than by the use of GCMs, but it is useful to first study results from a LAM simulation at a resolution roughly comparable to that of B95 to see if similar tropical cyclone–like vortices (TCLVs) are produced. There are two main requirements for a LAM if it is to simulate a realistic climatology of TCLVs compared to observations of tropical cyclones. First, the model must have a good simulation of the mean climate in the regions of interest, particularly of those parameters that are relevant to tropical cyclone formation (Gray 1975, 1979). We therefore examine the tropical climatology of the LAM to determine its quality. To diagnose the LAM's ability to generate tropical cy-

Corresponding author address: Kevin Walsh, CSIRO Division of Atmospheric Research, PMB1, Aspendale, Victoria 3195, Australia. E-mail: kevin.walsh@dar.csiro.au

clones, we employ Gray's Seasonal Genesis Parameter (SGP; see the appendix). The SGP is a parameter that uses seasonal-mean atmospheric fields and, when applied to observations, gives a reasonable simulation of the observed pattern of tropical cyclogenesis. While questions have been raised regarding whether all of the variables contained in the SGP are crucial or fundamental to tropical cyclone formation (e.g., Anthes 1982; Frank 1987; McBride 1995), we take the SGP as the starting point for our analysis as a comparison to previous work using this parameter. Using the SGP, Watterson et al. (1995b) showed that a global model demonstrated some skill in simulating observed variations in tropical cyclone numbers and formation regions, and it would be instructive to perform a similar analysis for the LAM. The SGP can then be compared to the model-generated climatology of TCLVs and the causes of any model deficiencies in this climatology thereby elucidated.

There must also be a method that enables TCLVs to be detected in the LAM that gives good results when observations are analyzed. Using such a method, TCLVs are reliably differentiated from other tropical low pressure systems using values of those atmospheric variables that are characteristic of real tropical cyclones. Ideally, such a method would use a set of criteria that, when applied to observations smoothed to the same resolution as the model, detects observed tropical cyclones (and only tropical cyclones). Walsh (1997) concluded that ECMWF analyses at a resolution of 1.125° of latitude were inadequate for establishing the values of such criteria because of data-sparse regions of the globe where real tropical cyclones were poorly analyzed. Here we use criteria that are based upon the structure of observed tropical cyclones at scales comparable to that of the model resolution and that have been successfully applied by Bengtsson et al. (1995) to produce realistic numbers and geographic distributions of TCLVs. We make some modifications to his criteria, which are described in the next section.

We wish to establish whether the TCLVs detected in the LAM resemble the observed characteristics of tropical cyclones, with particular emphasis on the following conditions:

1) genesis of TCLVs occurs at realistic locations and in realistic numbers,
2) the tropospheric structure of a composite TCLV resembles that of observed tropical cyclones,
3) the life cycles and tracks of TCLVs are similar to those observed, and
4) the distribution of TCLV intensities is similar to observed.

Here we define a ''tropical cyclone'' as a nonfrontal synoptic-scale low pressure system over tropical or subtropical waters with organized convection and definite cyclonic surface wind circulation (Holland 1993). A tropical cyclone with maximum sustained surface winds of less than 17 m s^{-1} is called a ''tropical depression,'' while a tropical cyclone with winds between 17 and 33 m s^{-1} is called a ''tropical storm.'' Stronger tropical cyclones are called ''hurricanes'' or ''typhoons.''

The main purposes of this paper are therefore to examine the tropical climatology of a LAM to determine its quality, particularly the simulation of those parameters relevant to tropical cyclone formation, and then to determine the characteristics of TCLVs generated by the model. The simulations so analyzed are those of Walsh and McGregor (1995). We also compare the vortices generated by the forcing GCM to those simulated by the LAM and show that those generated by the LAM are much more realistic. Section 2 describes the model and methodology of this study. In section 3, the results are presented, section 4 gives some discussion, and section 5 summarizes the conclusions of the study.

2. Model and methodology

The nested model DARLAM has been developed for both mesoscale studies and for climate change experiments. The model is a two-time-level, semi-implicit, hydrostatic primitive equations model; it uses an Arakawa staggered C grid and semi-Lagrangian horizontal advection with bicubic spatial interpolation. An earlier version was described by McGregor (1987). In the present experiments the model uses one-way nesting with lateral boundary conditions specified from the Mark I CSIRO nine-level R21 GCM (McGregor et al. 1993), which has evolved from the flux-conserving GCM of Gordon (1981). DARLAM uses a Lambert conformal projection and here has the same vertical level assignments as the GCM (nine sigma levels are used for both). The 77 × 77 domain with 125-km grid spacing used in this study is shown in Fig. 1. The topography of DARLAM is also shown in Fig. 1. DARLAM uses a modified version of the Kuo (1974) cumulus convection scheme, as well as a diagnostic cloud scheme. More detail on the physical parameterizations and numerics of the LAM is contained in Walsh and McGregor (1995).

The LAM results analyzed here consist of 10 separate 30-day simulations for January, where the boundary conditions of the LAM are supplied by the GCM; the average of the 10 simulations constitutes the model climatology. Climatological-mean sea surface temperatures are used for simplicity. There may be some effect on the results if interannually varying SSTs were specified, as there may be some nonlinear dependence of TCLV formation and intensity on SST. The 30-day simulations incorporated both diurnal and seasonally varying radiation but were initialized separately with output fields taken from a 10-yr seasonally varying run of the GCM; no vertical-mode initialization was performed, however. Tropical cyclones are frequently observed in January in the Australasian region (e.g., Watterson et al. 1995b), so it is of interest to analyze a DARLAM climate simulation of this month for the presence of

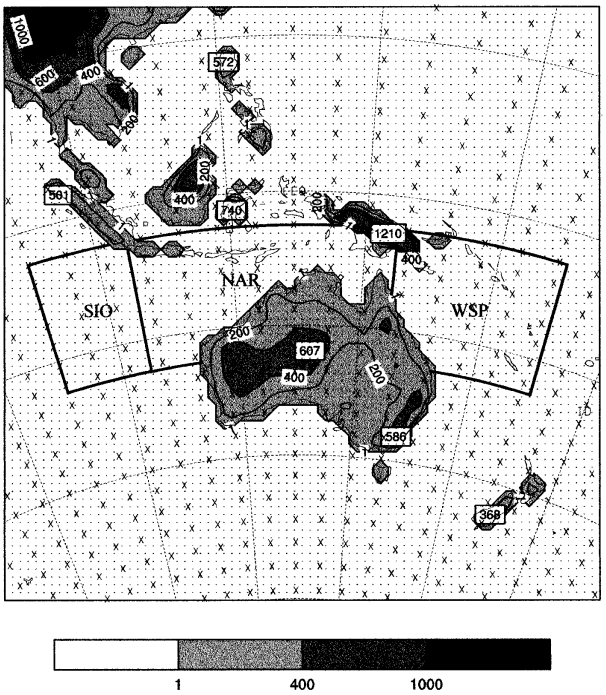

FIG. 1. DARLAM domain. Dots are DARLAM model grid points; crosses are GCM Gaussian grid points. Shown are tropical cyclone formation regions: South Indian Ocean (SIO), North Australian (NAR), and west South Pacific (WSP). DARLAM topography is also shown; contour interval is 200 m.

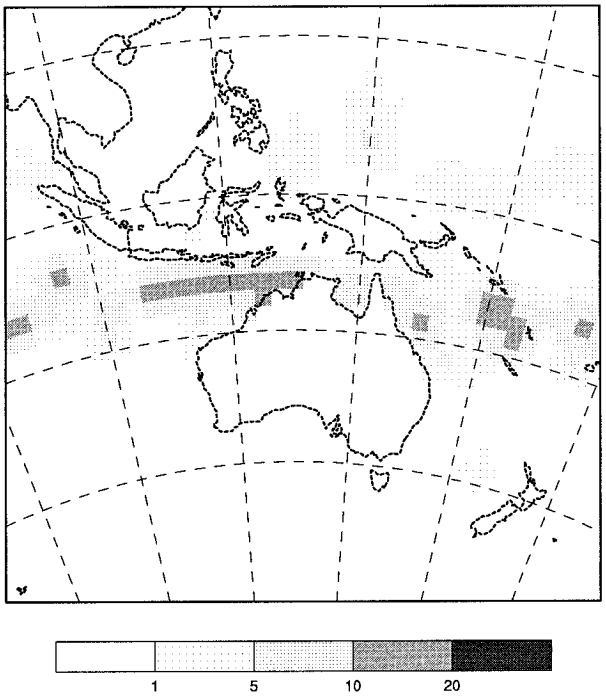

FIG. 2. Observed numbers of tropical cyclone genesis for January, for the period 1967–86. Contours are 1, 5, 10, 20 events per 5° square per 20 seasons (January numbers are multiplied by 3 to obtain equivalent seasonal numbers; values are interpolated to a 2.5° grid for clarity). Extracted from data supplied by NOAA (1994).

TCLVs. Figure 2 shows the observed numbers of tropical cyclones forming over the model domain in January, during the period 1967–86. Gray's SGP is scaled to units of genesis events per 5° grid squares per 20 seasons; the observations are shown in these units, where the derived numbers for January have been multiplied by 3 to obtain equivalent seasonal numbers for later comparison to Gray's SGP, and have been interpolated to a 2.5° grid for better comparison with model fields. Figure 2 shows that cyclogenesis is observed in a broad band east and west of the north coast of Australia. There is also a less intense band of cyclogenesis in the Pacific north of the equator, where some tropical cyclones form in this month despite the unfavorable season in the Northern Hemisphere. The apparent cyclogenesis west of New Zealand is caused by one storm very early in the data record and may be unreliable.

The daily fields of model output were examined using the method of Walsh (1997), which is largely based upon that of B95, with some minor differences. Briefly summarized, this method uses an objective technique to determine minimum threshold values of atmospheric variables that are characteristic of real tropical cyclones on the model grid used in the simulation analyzed. The main variables used for this purpose are the vorticity at 850 hPa (VORTMIN), the 10-m wind speed (W10MIN), and a midtropospheric temperature anomaly (TTOT) calculated over the center of the storm; we call these variables the detection criteria. We assume, in agreement with the definition of a tropical cyclone, that the TCLV must have a substantial cyclonic vorticity (VORTMIN $= 2.0 \times 10^{-5}$ s^{-1}). Little change in the number of detected TCLVs was found if this value was reduced to 5.0×10^{-6} s^{-1}, although numbers were considerably reduced when higher values of VORTMIN were applied. The chosen value of VORTMIN therefore appears to be an appropriate threshold. In our analysis, a threshold value of the maximum 10-m wind speed of a storm was also applied but examined alongside a criterion measuring area-averaged wind speed, which is described below. The 10-m wind speed was calculated using Monin–Obukhov similarity theory from a lowest dynamical sigma level of 0.979. The absence of a representation of the atmospheric boundary layer in the model would be expected to significantly affect the model's estimate of low-level wind speed, although this is likely a secondary consideration in a simulation of coarse horizontal resolution that does not resolve the eyewall of the cyclone. For TTOT, it was found that almost all of the tropical lows detected above a certain (low) minimum wind speed had positive TTOT values, so the TTOT threshold was simply set equal to zero. Both land and ocean points were examined; few storms were found to travel far inland before weakening, and no persistent low pressure systems over land (such as heat lows) were detected.

Additional minor criteria imposed are that the temperature anomaly at 300 hPa must be greater than that at 850 hPa and the wind speed over a region around the center of the storm must be greater at 850 hPa than at 300 hPa. This structure is clearly observed (Frank 1977). Removal of these structure criteria caused almost no change in the number of detected tropical low pressure systems having W10MIN = 10 m s $^{-1}$ but greatly increased the number of such detected systems in the subtropical and midlatitude regions. The chosen criteria are therefore selective rather than restrictive; in other words, we are not tuning the numbers of detected TCLVs by choosing values of the detection criteria that are different from an observed threshold for tropical storms. An additional criterion was imposed that requires that a particular storm should satisfy the imposed detection criteria for a minimum of 2 days, effectively eliminated all remaining midlatitude detections while only eliminating a couple of tropical lows.

One difference from the method of B95 is that here we also apply a threshold criterion based upon an area-averaged tangential wind speed, the mean outer core 10-m wind strength (OCS, Weatherford and Gray 1988a). This is the mean tangential wind speed at a height of 10 m in the region 1°–2.5° of latitude from the center of the storm. We apply this additional criterion for the following reason. The resolution of the LAM simulation (125 km) is coarser than the typical spatial scale of maximum winds in observed tropical cyclones: the radius of such winds from the center is typically 10–100 km (Anthes 1982). Thus the observed maximum wind speeds are subgrid-scale phenomena in the simulations analyzed here. Also, observations show that except for tropical cyclones of tropical storm strength or weaker there is little relationship between maximum wind speed and the OCS for individual storms (Weatherford and Gray 1988b). The OCS criterion does give a useful threshold for these weaker systems, however. The use of an OCS criterion enables comparisons of resolvable model wind speeds to observations at the same resolution. Nonetheless, we will also show that the maximum 10-m wind speeds at individual grid points in the TCLVs have a different spatial scale from those observed in tropical cyclones, and thus we also perform a comparison of these wind speeds to observations.

An estimate of an appropriate OCS threshold value can be obtained from the results of Weatherford and Gray (1988b), who present data showing the variation of OCS with storm intensity (their Fig. 1). Here a tropical storm in the Pacific is defined as one with a central mean sea level pressure less than 997 hPa (Atkinson and Holliday 1977). At a threshold OCS of 10 m s^{-1}, only about 10% of all storms of at least tropical storm strength would be missed, while weaker tropical systems would largely be excluded. Weatherford and Gray (1988a) state that the dataset that they analyzed consisted of almost all tropical cyclones in the analysis period, which lends weight to this argument. While these data were compiled for storms in the western North Pacific, where tropical cyclones are both more numerous and can reach greater intensities than in the regions adjacent to Australia, in the absence of similar data for the Australian region, we use the above OCS threshold for validation of the DARLAM climatology of TCLVs. We also examine storms with lower OCS values, under the assumption that being more numerous they would provide us with a better indication of the pattern of cyclogenesis.

In addition to describing the climatology of TCLVs in DARLAM, we compare this climatology to the expected numbers of tropical cyclones determined from the mean model fields based upon the SGP of Gray (1975). We can thus compare the SGP to actual cyclogenesis in order to compare the predictive ability of the SGP to that of the model in this context. The model's simulation of the various factors that make up the SGP is also examined in order to quantify the contribution made by each factor.

3. Results

a. January tropical climatology of the LAM

Walsh and McGregor (1995) examined the surface climate of the model in some detail for the simulation presented here. For the purposes of this study, we concentrate on the model's simulation of midtropospheric fields, as these are likely more relevant to the formation of tropical cyclones. We first compare the observed temperature structure in the tropical atmosphere to that of the model. Here we show the zonal mean calculated only over longitudes 100°–160°E and latitudes 30°S–15°N. These coordinates represent roughly the most extreme meridians in the Tropics and slightly farther south that are entirely contained within the DARLAM domain. Atmospheric stability in the tropical atmosphere is perhaps best expressed by the vertical profile of equivalent potential temperature, or θ_e (e.g., Emanuel 1994). Figure 3a shows zonal-mean θ_e for DARLAM, while Fig. 3b shows the difference of the DARLAM climatology minus the average of ECMWF analyses (at 2.5° resolution) for this month from 1985 to 1991 over the same region. The vertical structure is qualitatively similar in the LAM to the analyses. Maximum θ_e values are seen at low levels in the equatorial regions in both the model results and the analyses, and both have a saddle point in the midtroposphere near 700 hPa. There is a pronounced cool bias in the DARLAM results, particularly in the lower troposphere, however. This is a feature of the forcing GCM simulation also (Watterson et al. 1995a) and is a common problem in many global models (Boer et al. 1992; Hurrell 1995).

The relative humidity (which contributes to the θ_e field) is shown in Fig. 4. In general, there is good agreement in the relative humidity fields, except above the

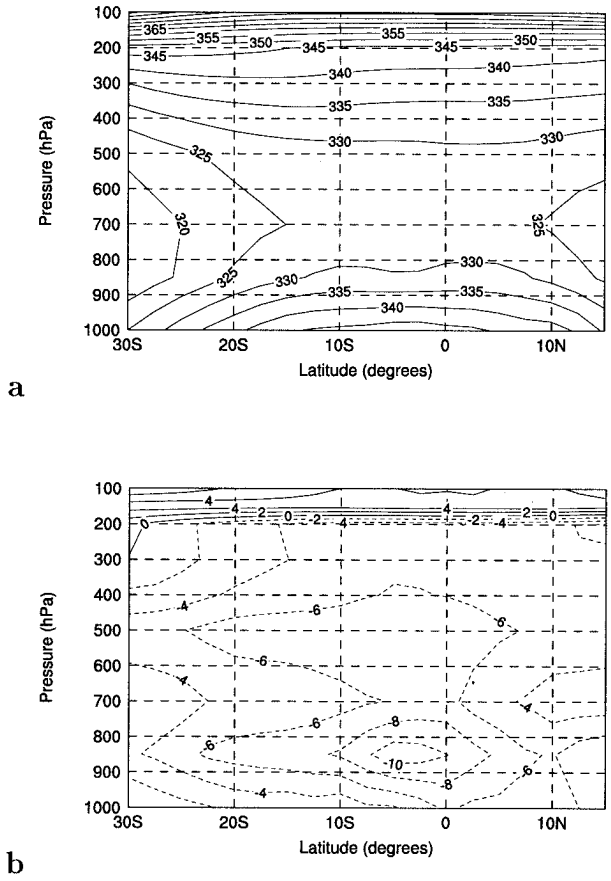

FIG. 3. January zonal-mean equivalent potential temperature as a function of pressure between longitudes 100° and 160°E, for (a) DARLAM climatology and (b) the difference of (a) minus the average of ECMWF analyses 1985–91. Contour interval is 5 K in (a) and 2 K in (b).

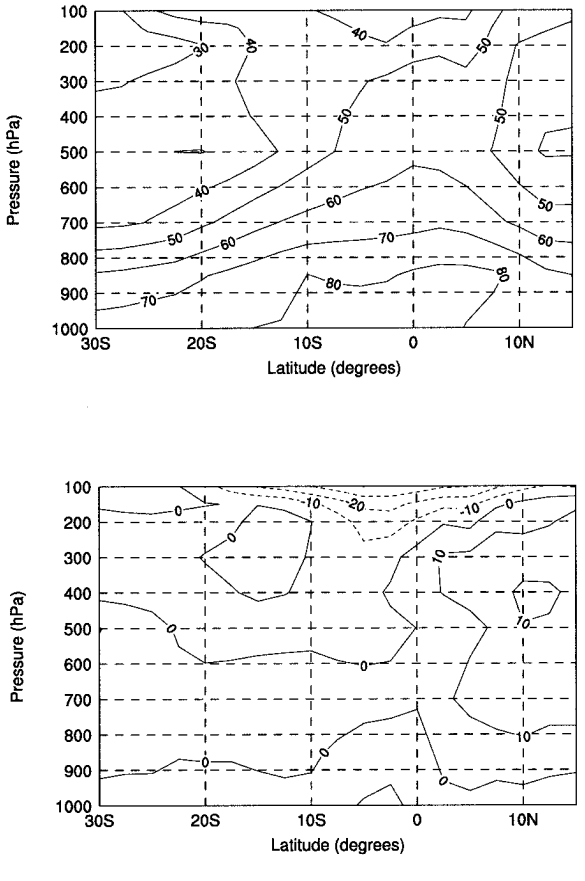

FIG. 4. January zonal-mean relative humidity as a function of pressure between longitudes 100° and 160°E, for (a) DARLAM climatology and (b) the difference (a) minus the average of ECMWF analyses 1985–91. Contour interval is 10%.

tropopause in the equatorial regions, where the model is too dry, and in the mid- and upper troposphere north of about 5°N, where the model is generally moister than the analyses. Otherwise the low-level and midtroposphere fields are generally similar to the analyses. The quality of the analyses themselves for this variable is an important issue (e.g., Trenberth 1992), and these results may be subject to revision as better data are obtained.

b. Model simulation of factors relevant to the formation of tropical cyclones

Here we examine the model's simulation of the parameters of Gray's SGP. In the simulation analyzed here, climatological SSTs are specified, so this is not a factor in any differences between the climatology of the LAM and the observations. The vertical lapse rate of the atmosphere is important because a more unstable atmosphere is thought to be more conducive to storm formation. The tropical atmosphere is largely unstable between these two atmospheric levels in both the LAM and the analyses (not shown). The area of instability extends farther south in the model than it does in the analyses, perhaps because the model is generally more unstable than the analyses over the ocean. This is true in most parts of the domain, with the exception of a region near the Philippines and near the eastern and western boundaries. The largest differences are seen off the north coast of Australia. This increased instability in DARLAM compared to the analyses is consistent with the specification of climatological SSTs in the model and the aforementioned cool bias in the model in the midtroposphere.

The midtropospheric relative humidity is also an important factor in tropical cyclone formation, with a more moist midtroposphere promoting the development of cyclones. Figure 5 shows the mean relative humidity between 700 and 500 hPa for the analyses and the model. Analyzed values (Fig. 5a) are largest over the equatorial regions, particularly the Indonesian region, which is a region of high observed rainfall (Legates and Willmott 1990). Low humidities are observed in the subtropical oceanic regions west and east of Australia; in this month, these regions are dominated by the subtropical

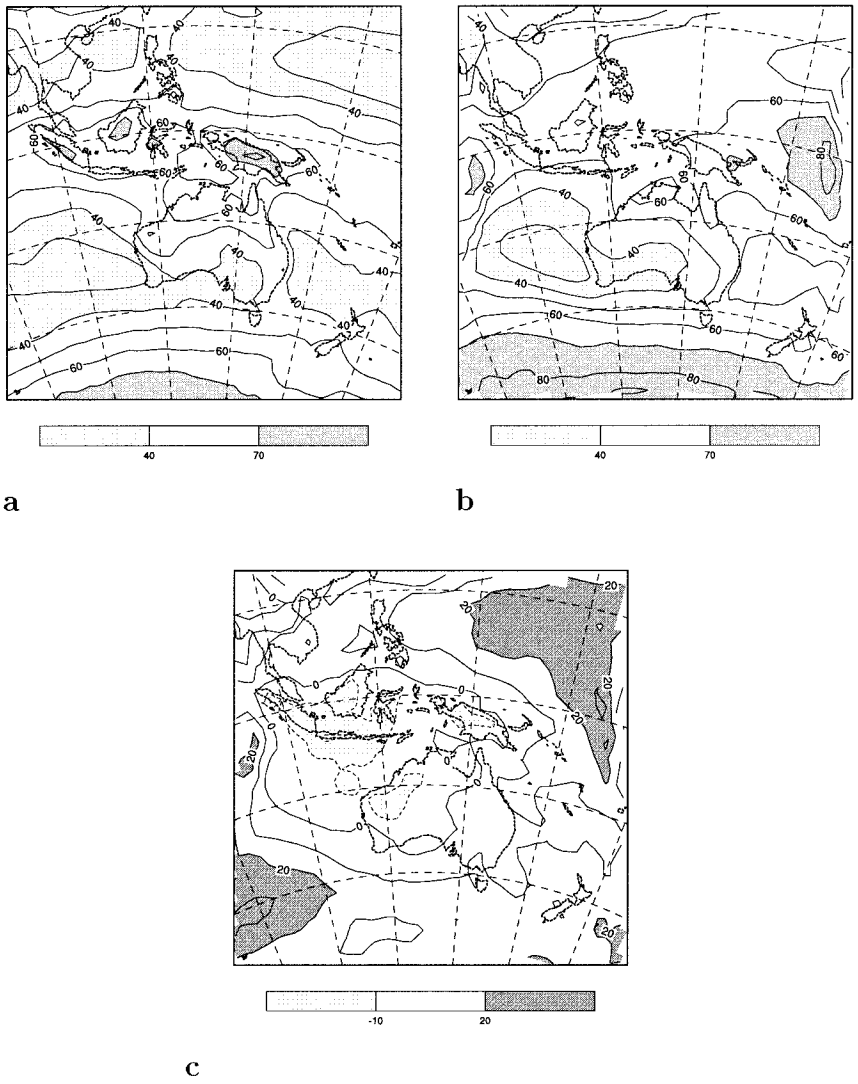

FIG. 5. January average relative humidity between 700 and 500 hPa for (a) average of ECMWF analyses 1985–91, (b) DARLAM climatology, and (c) the difference (b) minus (a). Contour interval is 10%.

high and convection is suppressed. The DARLAM simulation (Fig. 5b) also has low relative humidities in this region and mostly higher values at equatorial latitudes, but the differences (Fig. 5c) show that simulated humidities are rather lower than observed over Indonesia and the western parts of Australia and New Guinea. On the other hand, simulated humidities are higher elsewhere in the model domain. At equatorial latitudes, there appears to be some correlation in the model simulation between midtropospheric relative humidity anomalies and precipitation anomalies (not shown; see Walsh and McGregor 1995).

Vertical wind shear S_z is defined as in Gray's SGP:

$$S_z = \sqrt{(u_{950} - u_{200})^2 + (v_{950} - v_{200})^2}, \qquad (1)$$

where u is the zonal wind, v is the meridional wind, and the subscripts refer to pressure levels in hPa. Low values of S_z promote tropical cyclone formation. Simulated S_z (not shown) has a largely similar pattern to that observed, although the differences show that S_z is mostly larger in DARLAM than observed in the tropical regions of the model domain. In particular, largest differences occur near New Guinea. The orography of New Guinea is tall and narrow even at a relatively coarse resolution of 125 km (Fig. 1), and it was found in McGregor and Walsh (1993) that the specification of this orography strongly influenced the low-level flow.

Low-level (950 hPa) cyclonic vorticity is shown in Fig. 6. DARLAM's simulation of this variable is reasonable, but there are a few interesting differences. Of particular interest is the region near the eastern tip of New Guinea, where there is a local maximum of cy-

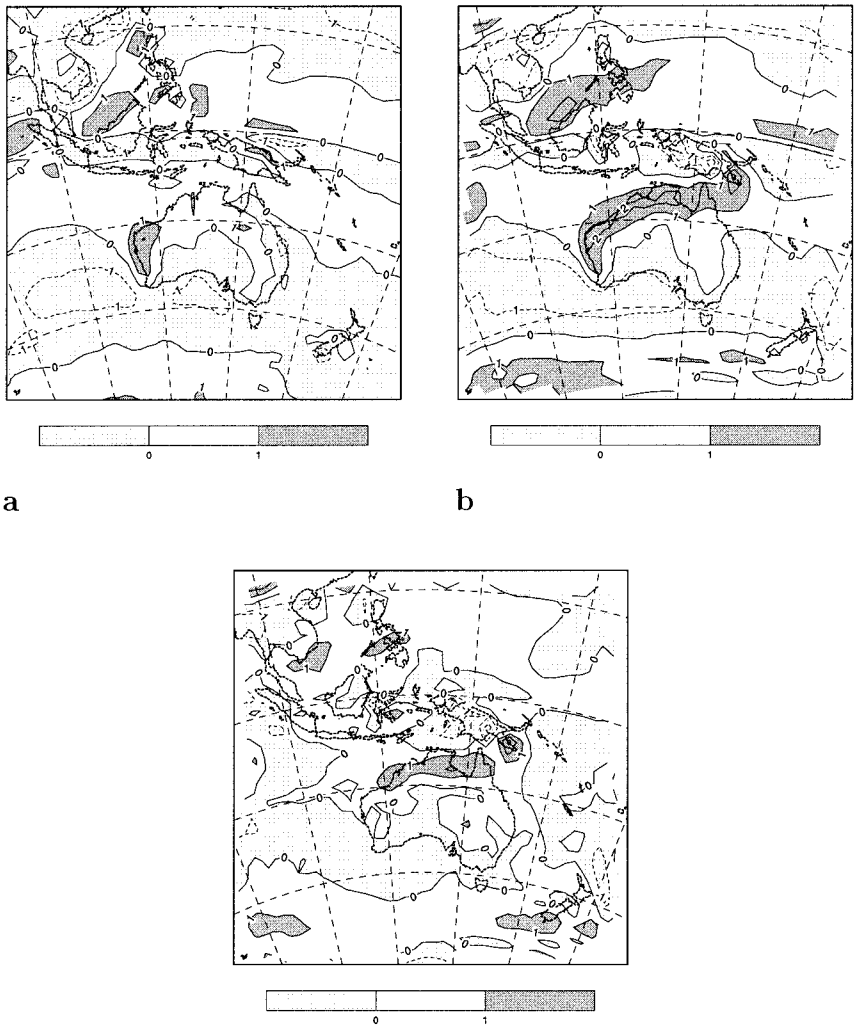

FIG. 6. January 950-hPa cyclonic vorticity for (a) average of ECMWF analyses 1985–91, (b) DARLAM climatology, and (c) the difference (b) minus (a). Contour interval is 1×10^{-5} s^{-1}.

clonic vorticity in the DARLAM simulation. This is again caused by orographically forced anomalous flow and is a major difference between the simulated and analyzed fields (Fig. 6c). Additionally, greater than observed cyclonic vorticity is seen along the northern fringe of Australia, caused by generally stronger wind gradients in this region in DARLAM. Regions farther east and west of the continent have lower than observed vorticities, however. Elsewhere in the Tropics, there appears to be little systematic pattern of difference, with the exception of a region in the South China Sea. This positive anomaly, like that seen near New Guinea, may also be topographically forced. This issue is discussed later in the paper.

In summary, factors in the DARLAM simulation that may tend to promote cyclogenesis relative to the observations are a more-unstable-than-observed low and midtroposphere in the areas of tropical cyclone formation and higher low-level vorticity. Factors that may act to reduce cyclogenesis include lower midtropospheric relative humidity northwest of Australia and generally higher wind shear immediately north of the continent (although it becomes lower farther south). In the next section, we discuss the characteristics of the TCLV cyclogenesis pattern in the DARLAM simulation and diagnose the reasons for it using Gray's SGP.

c. Genesis of TCLVs

We now use the methodology described in section 2 to count and identify TCLVs. We first examine the genesis locations and numbers of all TCLVs with a minimum OCS of at least 10 m s^{-1}, which as mentioned

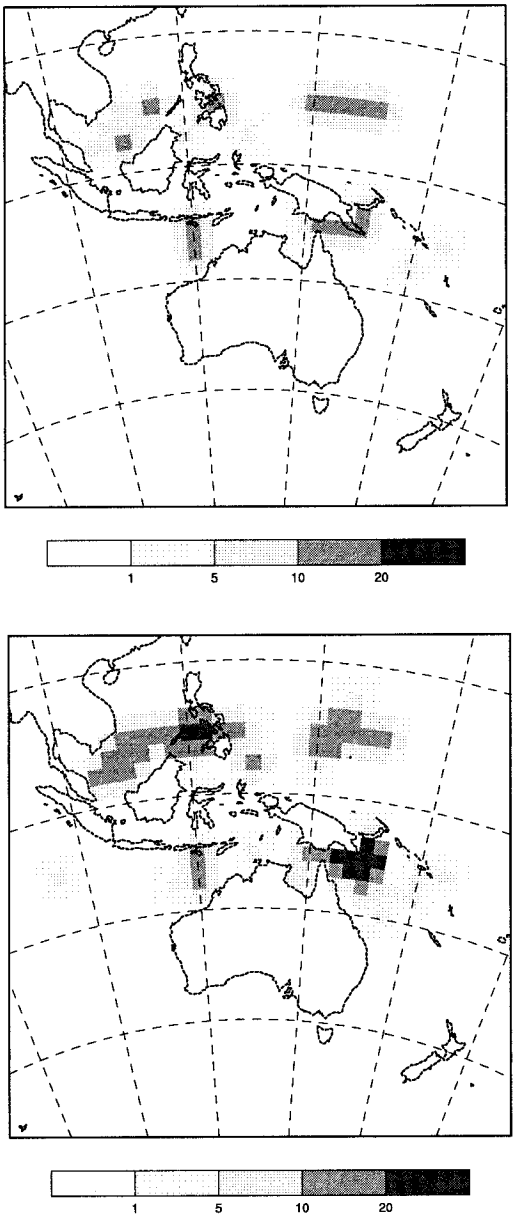

FIG. 7. Cyclogenesis for storms with an OCS of at least (a) 10 m s^{-1} and (b) 6 m s^{-1}. Contours are 1, 5, 10, 20 events per 5° square per 20 seasons; values are interpolated to a 2.5° grid for clarity.

earlier is a reasonable cutoff for tropical storms derived from observations.

Figure 7a shows the model genesis of such TCLVs for all storms with an OCS of at least 10 m s^{-1}, while Fig. 7b shows a similar plot for all storms with an OCS of at least 6 m s^{-1}. Figure 7b is displayed in order to give a better indication of typical cyclogenesis statistics than the fewer storms of Fig. 7a. With only 10 months of model output and fewer simulated storms, the model-simulated pattern of Fig. 7a is less well established statistically than that of Fig. 7b. Two characteristics of these results are of particular interest. The first is that there are few TCLVs formed to the west of the Australian continent apart from an area just off the northwest coast. This is predicted by the SGP (Fig. 8c) and probably caused by the low values of relative humidity simulated by DARLAM in this region. The second is the peak of cyclogenesis in the model just south of New Guinea, which is also predicted by the SGP. This local maximum is stronger than in reality and may be related to the higher than observed simulated cyclonic vorticity in this region shown in Fig. 6c. Pattern correlations (not shown) performed between the various components of the SGP and the model-generated pattern of cyclogenesis shown in Fig. 7b clearly demonstrate the dominating influence of the vorticity component.

Table 1 compares the numbers of TCLVs generated by DARLAM to observations and the SGP, for the different basins shown in Fig. 1. The north Australian region (NAR) basin extends over latitudes 25°–5°S and longitudes 105°–145°E, the west South Pacific (WSP) basin is bounded by the same latitudes but by longitudes 145°–170°E, and the south Indian Ocean (SIO) basin extends from 90° to 105E. These basin definitions are similar to those defined by the World Meteorological Organization (WMO), although only portions of the WMO-defined WSP and SIO basins are wholly contained within the DARLAM grid. In general, DARLAM underestimates observed numbers in basins near the Australian continent. In addition to the low relative humidity values discussed above, this result may also be related to the structure of the TCLVs compared to that of observed tropical cyclones, as discussed below. In contrast, DARLAM greatly overestimates the numbers of TCLVs formed in the North Pacific (see also Fig. 9). As shown by the SGP results (Table 1; Figs. 8b,c), conditions in both the LAM and the forcing GCM in the North Pacific for this month are much more conducive to tropical cyclone formation than they are in reality. There are a number of reasons for these results. Both the LAM (Fig. 5c) and the forcing GCM (not shown) have substantially higher midtropospheric relative humidities in this region than the analyses. Additionally, the proximity of this region to eastern boundary of the DARLAM domain creates anomalous rainfall patterns that strongly affect the relative humidity field in the LAM. These problems were noted by Walsh and McGregor (1995). It was also noted that the simulation of the mean surface climate was poor over the North Pacific region in both the LAM and the GCM; thus it is not surprising that the simulation of tropical cyclone genesis is also poor in this area.

Cyclogenesis in DARLAM is particularly large in the region of the South China Sea. In this region, the relative cyclonic vorticity is high (see Figs. 6b,c), which promotes cyclogenesis (e.g., McBride and Zehr 1981). Given that mean cyclonic vorticity values in this region are comparable to the threshold of vorticity used to define TCLV detection, it is not surprising that many such storms are detected. The climatology of DARLAM thus

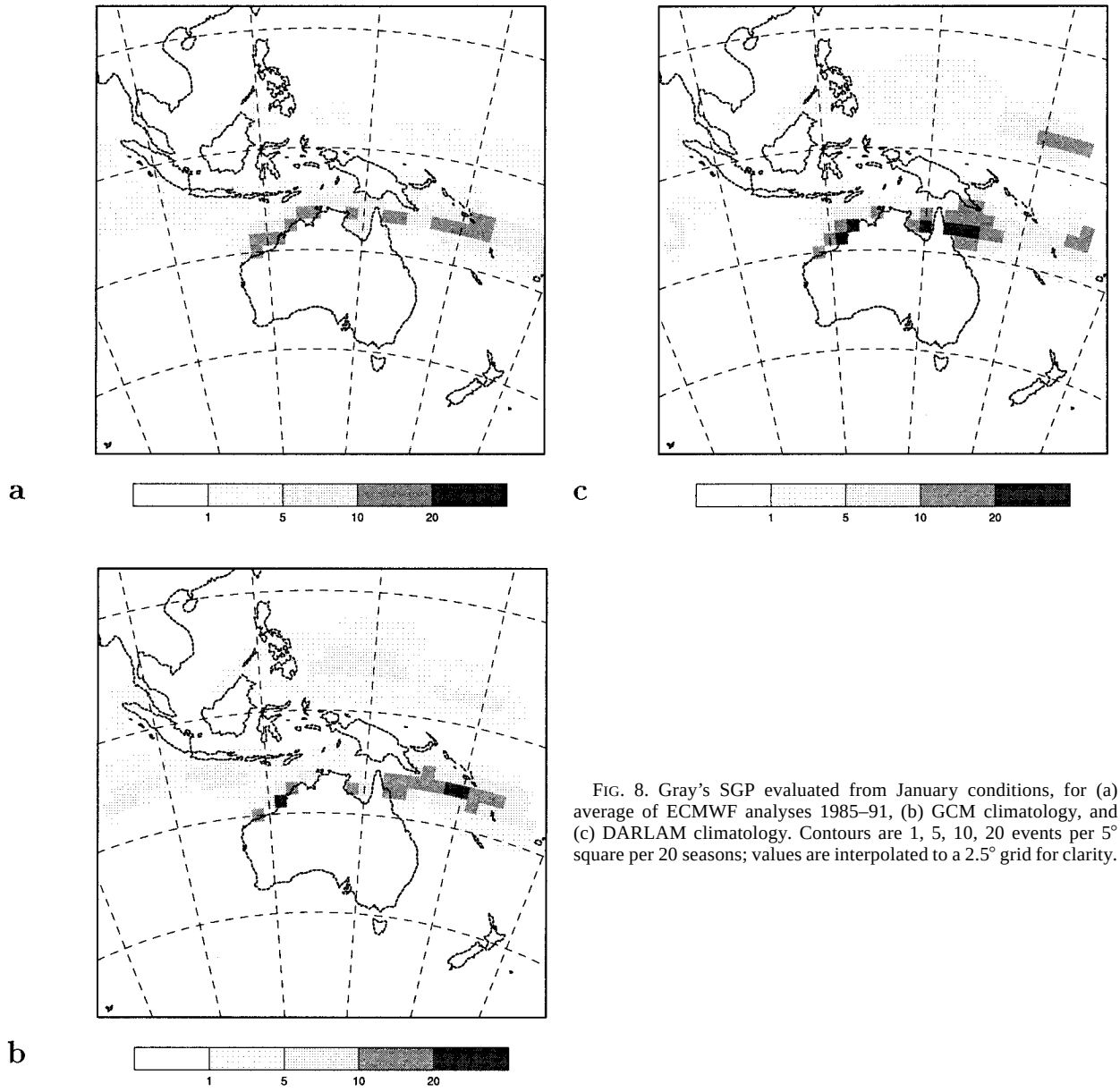

FIG. 8. Gray's SGP evaluated from January conditions, for (a) average of ECMWF analyses 1985–91, (b) GCM climatology, and (c) DARLAM climatology. Contours are 1, 5, 10, 20 events per 5° square per 20 seasons; values are interpolated to a 2.5° grid for clarity.

needs to be improved significantly in this region. The cause of the excess vorticity is probably related to anomalous forcing by the topography of the LAM; experiments conducted with the LAM in which topography was arbitrarily lowered in the surrounding land areas showed that the cyclonic vorticity anomaly was reduced in intensity.

Note that in this region the SST is generally lower than the threshold value used in the SGP (26°C), thus largely eliminating significant SGP values over this region (Fig. 8c). The fact that the SGP does not predict substantial cyclogenesis in this region while a considerable amount actually occurs in the model suggests that the SGP is only an approximate predictor of TCLV gen-

TABLE 1. Number of tropical storms and hurricanes per season predicted by the SGP using January ECMWF and DARLAM fields compared to observations and DARLAM model output (scaled to the same units) over the various basins.

Source	NAR	WSP	N. Pacific	S. Indian
ECMWF SGP	3.4	3.4	0.5	1.5
GCM SGP	3.0	4.2	2.9	1.7
DARLAM SGP	3.8	4.6	2.8	1.2
Observed	4.0	3.6	0.8	3.0
DARLAM model	2.1	2.7	5.7	0.0

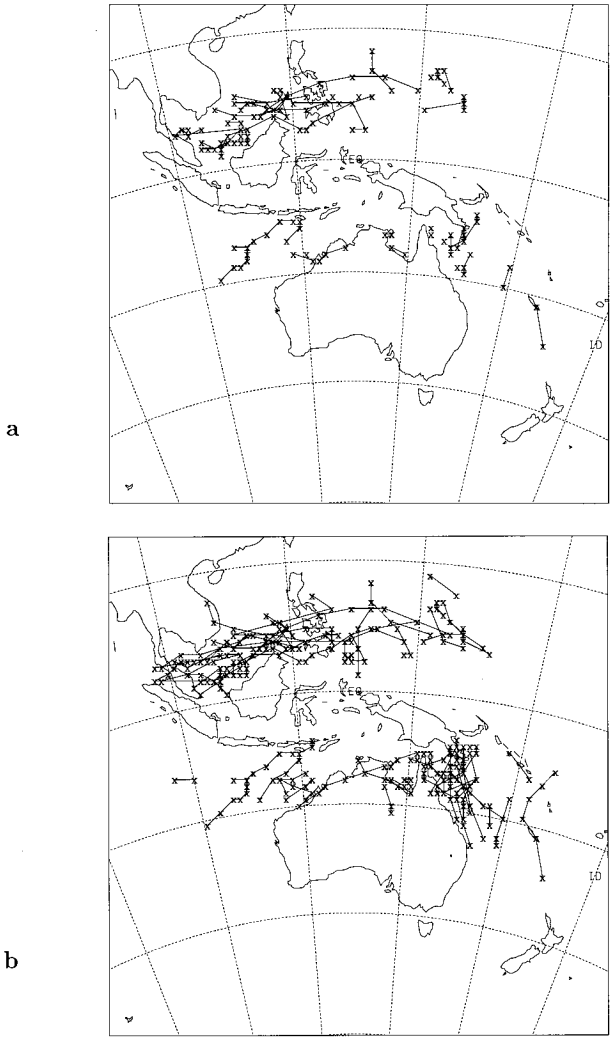

FIG. 9. DARLAM January simulation of occurrence and tracks of TCLVs with an OCS of at least (a) 10 m s^{-1} and (b) 6 m s^{-1}.

esis, at least in regions where the cyclonic vorticity is large. Watterson et al. (1995b) also found discrepancies between cyclogenesis predicted by the SGP and that observed. While the results of Table 1 suggest that the SGP as applied to the ECMWF analyses gives reasonable results compared to observations, the comparison between the DARLAM SGP and the actual TCLV cyclogenesis in the model is only approximate, with the SGP only giving a broad indication of likely variations in numbers. For example, the DARLAM SGP in the North Pacific is much larger than the observations, but it is only within about a factor of 2 of the actual DARLAM cyclogenesis.

Similarly, Table 2 shows pattern correlations between the model-generated SGPs, the observations, and the DARLAM cyclogenesis over the Southern Hemisphere portion of the DARLAM domain; these also show only approximate predictive ability for the SGP. First, the pattern correlation between the DARLAM cyclogenesis

TABLE 2. Pattern correlations of SGP derived from model and analyses with observed and DARLAM cyclogenesis (0°–30°S, 90°–170°E).

Source	DARLAM SGP	Observed
ECMWF SGP	—	0.53
GCM SGP	—	0.58
DARLAM SGP	—	0.40
DARLAM cyclogenesis (OCS $>$ 10 m s^{-1})	0.27	0.26
DARLAM cyclogenesis (OCS $>$ 6 m s^{-1})	0.41	0.33

of Fig. 7b and the observations in this region is modest, with a value of 0.33. The ECMWF SGP has reasonable agreement with the observations, but the GCM SGP correlation is actually higher. Watterson et al. (1995b) showed that the ECMWF fields exhibited less than perfect skill at predicting cyclogenesis patterns using the SGP, and they attributed this result to uncertainties in the specification of the humidity fields in these analyses (see also Trenberth and Guillemot 1995). Additionally, the DARLAM SGP correlation is lower than that of the GCM SGP, which suggests that the GCM is simulating somewhat more realistic large-scale fields than the LAM, at least those that are considered crucial for tropical cyclogenesis. But the SGP is also not a perfect predictor of model-generated cyclogenesis when working on DARLAM output, as there is only marginal agreement (a correlation of 0.41) between the pattern predicted by the DARLAM SGP (Fig. 8c) and that of the model cyclogenesis shown in Fig. 7b. These results suggest that while the SGP may be useful to diagnose whether the large-scale forcing of a GCM is likely to contribute to poor cyclogenesis results in a LAM, the SGP is less useful as a detailed predictor of model cyclogenesis patterns. While the SGP might show more skill if a longer model simulation were performed, it is likely that a reformulation of this parameter may in the future provide a better climatological estimate of cyclogenesis, both model generated and observed.

d. Tracks and life cycles of TCLVs

This section illustrates the life cycle of a typical TCLV and demonstrates that its life cycle has certain similarities to reality. Figure 9a shows TCLV tracks and locations for all storms with an OCS greater than or equal to 10 m s^{-1}, the genesis locations of which are shown in Fig. 8a, while Fig. 9b shows the same for all storms with an OCS of at least 6 m s^{-1} (cf. Fig. 8b). Some storms in Fig. 9a spent only 1 day above the OCS threshold of 10 m s^{-1}, but were clearly present for several days in the track data at a threshold of 6 m s^{-1}, and so are included. No midlatitude systems were present at either threshold for more than 1 day. Tracks are generally similar in character to observed tropical cyclone tracks in this region, while the regions of TCLV oc-

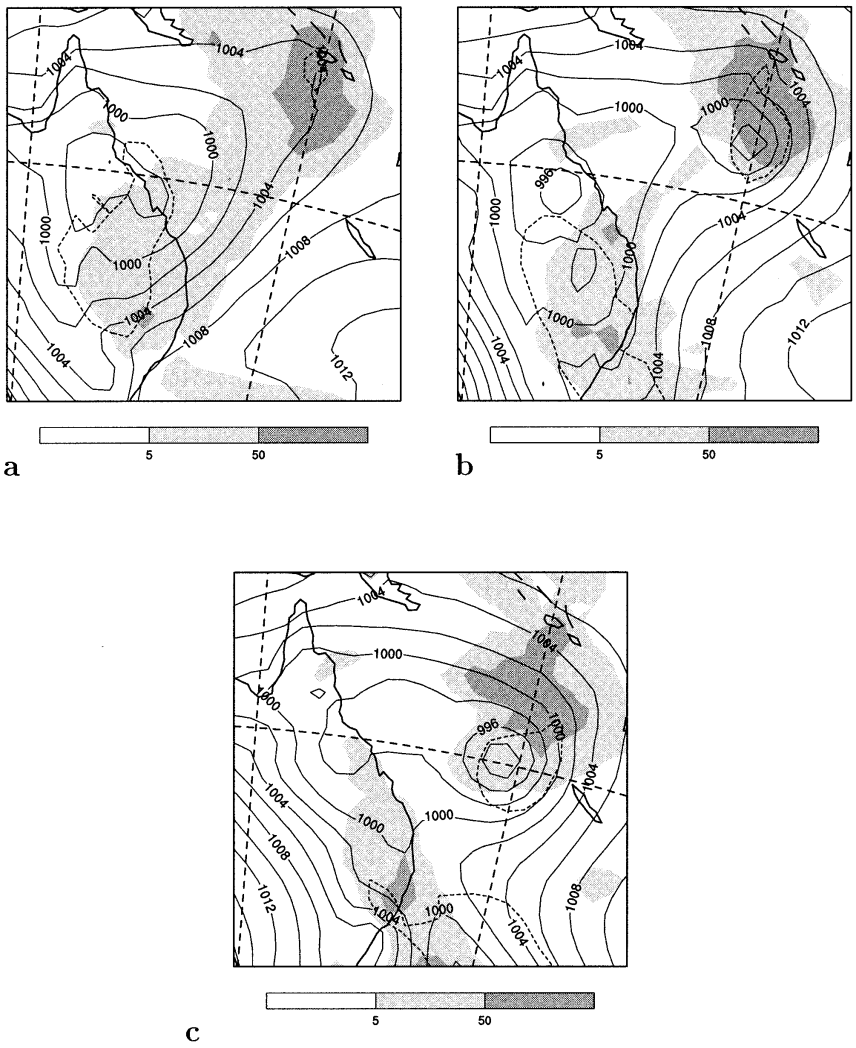

FIG. 10. TCLV as simulated by DARLAM, in a region off the Australian coast, for (a) day 11 of simulation, (b) day 12, and (c) day 13. Solid contours are mean sea level pressure, dashed line is edge of region where midtropospheric temperature anomaly is greater than 2°C, and shading is precipitation. Contour interval for mean sea level pressure is 2 hPa, and variable contour interval for precipitation, in millimeters per day: (d) day 14 of simulation, (e) day 15, and (f) day 16.

currence are also similar to observed, except in the North Pacific region (e.g., Elsberry 1995).

Figure 10 shows a series of plots that detail the life cycle and some of the features of a typical intense TCLV. This storm formed in the model simulation off the coast of northeastern Australia and subsequently traveled southward. The figures are shown at 0400 UTC for successive days, from the day before the cyclone formed to its apparent transition to an extratropical system.

One day before the TCLV formed (day 11 of the 30-day simulation, Fig. 10a), the synoptic situation was characterized by a broad trough of surface low pressure extending north-eastward from the Australian coast. Considerable convective activity was associated with this trough. Figure 10b shows the TCLV soon after formation, when it was located several hundred kilometers northwest of New Caledonia. The TCLV had a closed circulation, a warm core, and was associated with intense convection. Maximum 10-m wind speeds at this time were 17 m s^{-1}, while the OCS was 11 m s^{-1}. By day 12 (Fig. 10c), the TCLV had moved south; the warm core had weakened somewhat by this time, the 10-m maximum wind speed had stayed constant at around 17 m s^{-1}, while the OCS had declined to 10 m s^{-1}. The storm continued to move southward and weaken slightly by the next day (Fig. 10d), and it may have begun to recurve near this time. The 10-m wind speed had declined to 14 m s^{-1}, and the OCS to 9 m s^{-1}. By day 15 (Fig. 10e), the storm was no longer axisymmetric, a sign that it was adopting extratropical characteristics (Anthes 1982). Finally, the storm lost its identity as it merged with a midlatitude cold front (Fig. 10f). These figures show that a typical intense TCLV has a life cycle

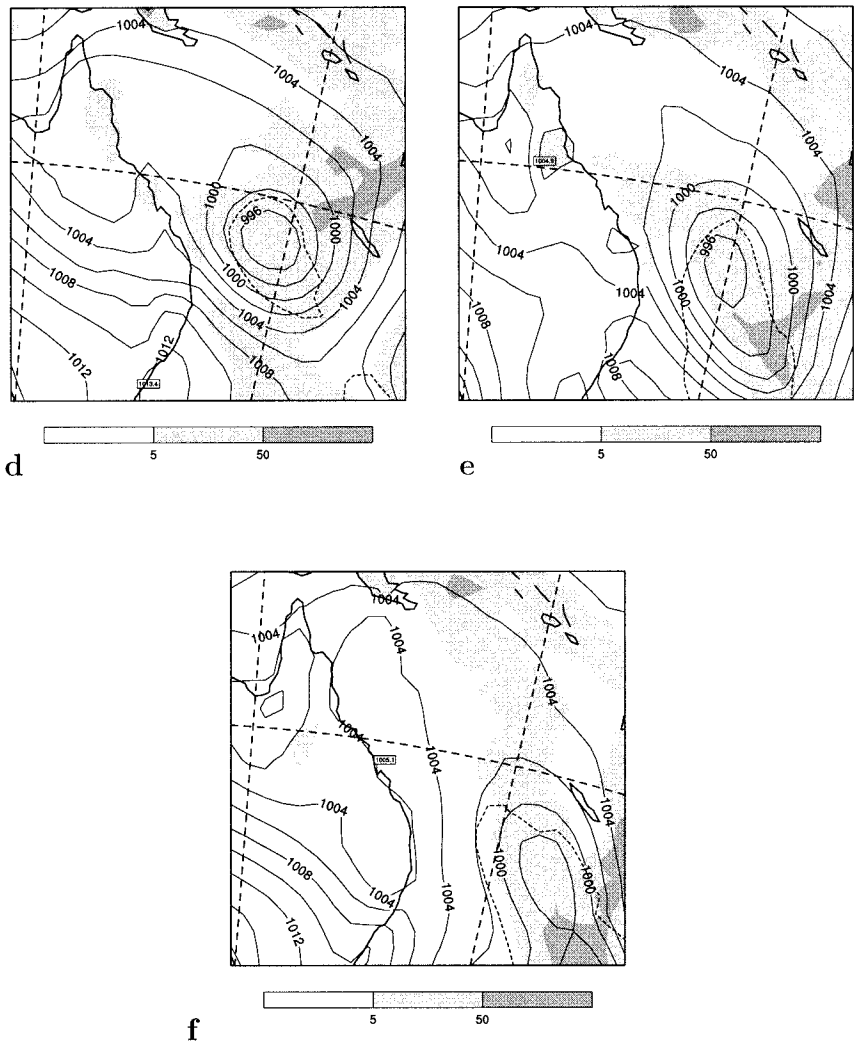

FIG. 10. (*Continued*)

and a track that is similar in many respects to that of a real tropical cyclone.

The mechanisms of cyclogenesis for this storm are examined in Fig. 11. The characteristics of the vorticity and divergence structure of the precyclone and cyclogenesis stages of the TCLV are important to show whether its formation mechanisms resemble those of observed tropical cyclones. Here we show the vertical structure 1 day before development (day 11, cf. Fig. 10a) and on the first day of development (day 12, cf. Fig. 10b). In the absence of a closed low pressure system on day 11, the center of the predevelopment system was taken to be the maximum in the 1000-hPa vorticity field, about 200 km northeast of the position of the developed storm on the next day. In the predevelopment stage, the storm already has a substantial tangential wind speed (Fig. 11a) and vorticity (Fig. 11c). There is a deep layer of cyclonic vorticity through the entire troposphere, which Tuleya (1988) found to be a characteristic of developing tropical cyclones. The ratio of the radial velocity (Fig. 11b) to the tangential velocity below about 400 hPa is slightly larger than typically observed in tropical weather systems (e.g., Ruprecht and Gray 1976), but Davidson and Kumar (1990) found similar ratios in their simulation of the development of Tropical Cyclone Irma using a high-resolution (50 km) regional model. The predevelopment disturbance also has a warm core in the midtroposphere (see Fig. 10a), although the vorticity profile indicates that it has a cold core below the vorticity maximum at about 700 hPa. This structure is usually a feature of storms 2–3 days before formation (McBride 1995), somewhat earlier than the system shown here.

In the early development stage (Fig. 12), the tangential wind velocity increases and the maximum moves toward the surface, as does the maximum region of relative vorticity, which descends to about 900 hPa. This movement of the vorticity maximum toward the surface is observed in developing systems (Da-

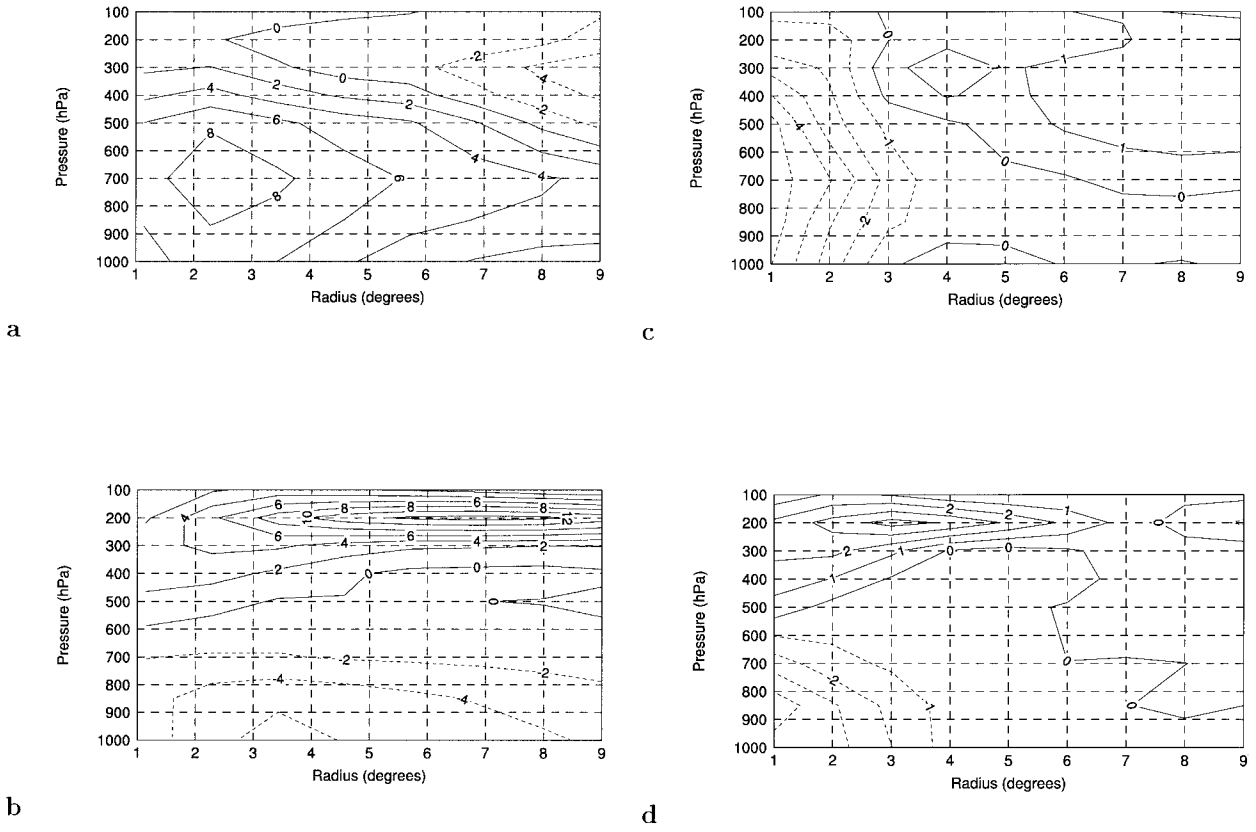

FIG. 11. Vertical profile (pressure in hPa vs radius from storm center in degrees of latitude) of predevelopment storm on day ll of DARLAM simulation, for (a) tangential velocity, (b) radial velocity, (c) vorticity, and (d) divergence. Contour intervals are 2 m s^{-1} for (a) and (b), 10^{-5} s^{-1} for (c) and (d).

vidson et al. 1990; McBride 1995) and indicates that the disturbance now has a warm core throughout the troposphere (see also Fig. 10b), which is a feature of developing tropical cyclones (McBride 1995). The structure of the developed TCLV and predevelopment system are also similar in many respects to that shown for Hurricane Frederic by Krishnamurti et al. (1994) in their simulations using a high-resolution (T170) global spectral model.

We have also performed a simulation of this storm at a horizontal resolution of 30 km. This run was one-way nested within the 125-km simulation over a small domain off the northeast coast of Australia; thus it is a multiply nested simulation. It was commenced at day 10, that is, 1 day before Fig. 10a, and cyclogenesis occurred at roughly the same time and location as shown in Fig. 10b for the 125-km resolution run. Table 3 shows a comparison between the two simulations. Minimum central pressures and maximum 10-m wind speeds were generally more intense in the 30-km simulation, as expected. The smaller size of the storm in the 30-km run at day 12 led to a lower OCS, even though the maximum 10-m wind speed was higher; OCS values increased when the storm became larger as it moved south, a feature of observed tropical cyclones (Anthes 1982). Maximum wind speeds in the 30-km simulation occurred closer to the center of the storm than in the 125-km simulation (cf. Figs. 12a and 12e), which is more realistic (cf. Fig. 14). As the storm moved southward (not shown), it followed a track quite similar to that seen in Fig. 10.

Estimated mean lifetimes of observed tropical cyclones are compared to those of simulated TCLVs in Table 4. Simulated lifetimes (defined as the average number of days that the TCLV had an OCS of at least 10 m s^{-1}) are lower in the WSP region and higher in the NAR region than observed. Because of the relatively small number of TCLVs generated using only 10 months of model output, at the present time it is only possible to say that the TCLV mean lifetimes in the Southern Hemisphere are not unrealistic.

e. Composite structure of TCLVs

We wish to compare the mean structure of TCLVs to the observed structure of tropical cyclones. As mentioned in section 2, the detection criteria are chosen so as not to constrain the structure of TCLVs (and thereby their composites), but rather to exclude from consideration other, higher-latitude lows with a different struc-

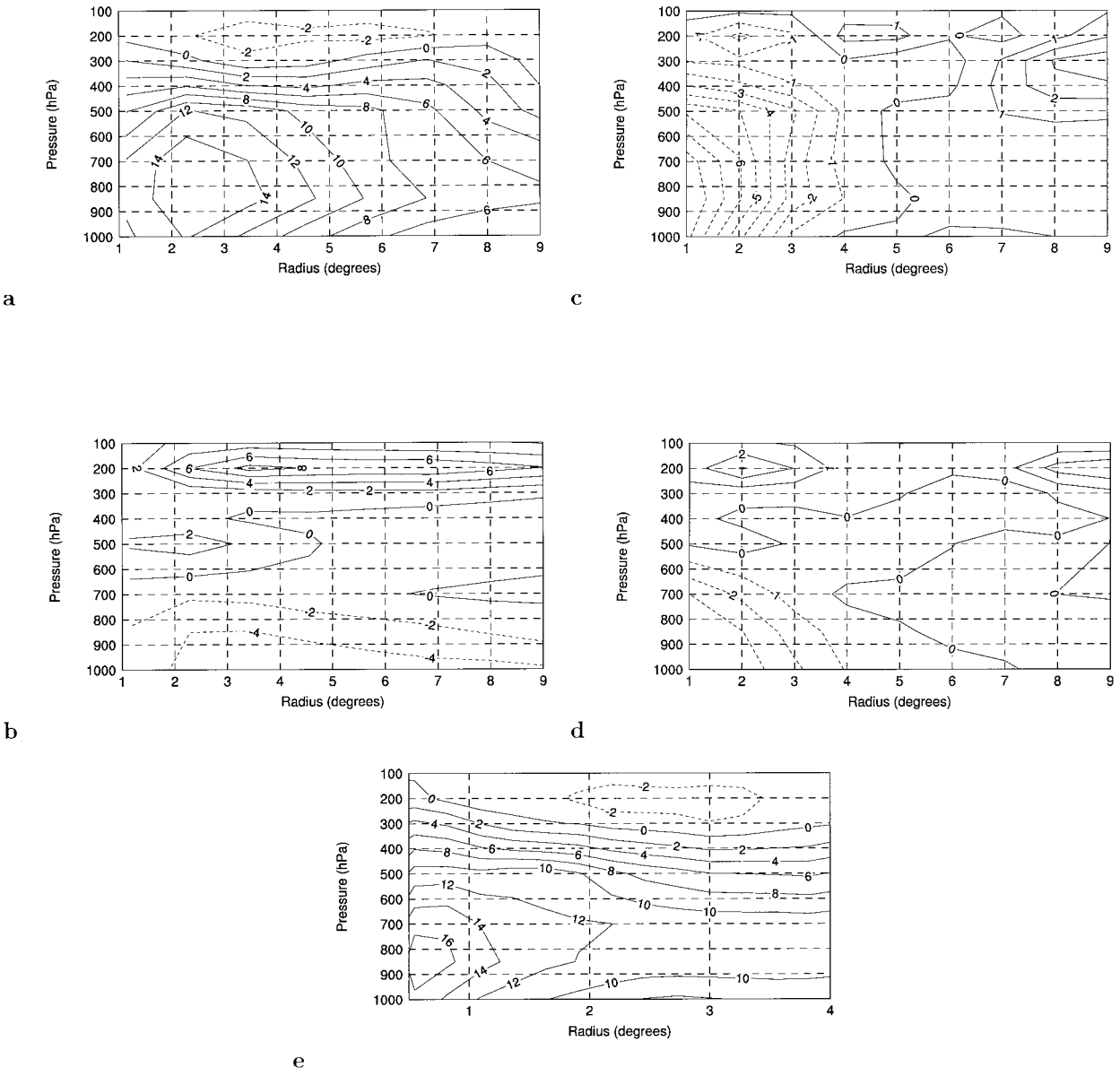

FIG. 12. The same as Fig. 11 for day 12 of DARLAM simulation, for (a) tangential velocity, (b) radial velocity, (c) vorticity, and (d) divergence; and (e) the same as (a) for the multiply nested 30-km simulation. Contour intervals are 2 m s^{-1} for (a), (b), and (e); and 10^{-5} s^{-1} for (c) and (d).

ture. In the North Pacific, the surface climate of DARLAM, the predicted SGP numbers from the DARLAM simulation, and the actual numbers of TCLVs generated by the model are not good, so in subsequent analyses

TABLE 3. Comparison of TCLVs simulated at 125-km and 30-km resolutions.

Day	Minimum pressure		Maximum 10-m wind speed		OCS	
	125	30	125	30	125	30
12	996	995	16.7	21.2	11.1	9.0
13	993	991	16.7	19.0	10.3	10.2
14	994	989	14.0	15.6	8.9	12.6
15	995	986	12.7	19.6	6.8	13.8

TABLE 4. Estimated mean lifetimes of tropical storms and hurricanes in two basins compared to DARLAM TCLV lifetimes, in days per storm.

Source	NAR	WSP
Observed	3.0	5.0
DARLAM	3.9	2.2

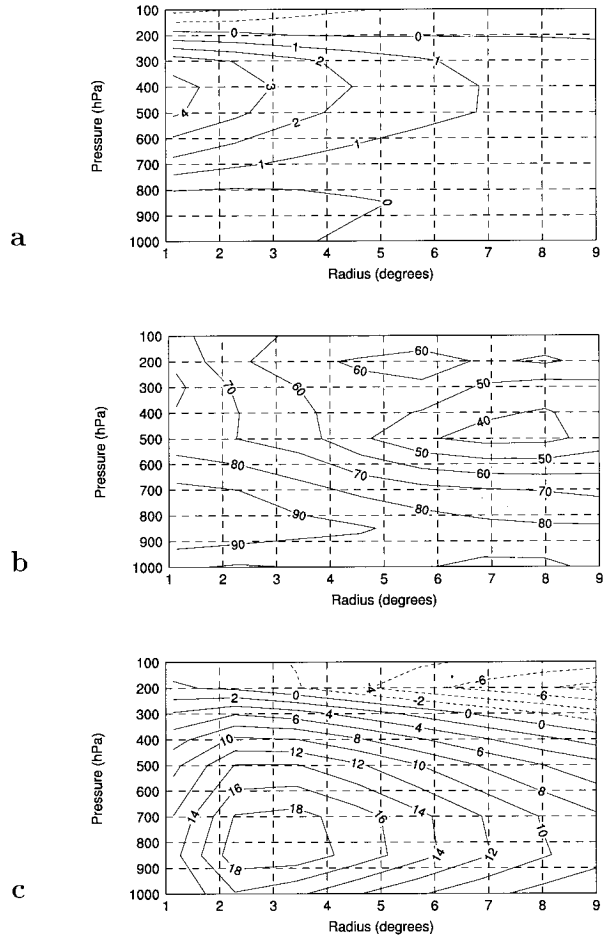

FIG. 13. Composite TCLV structure for all of the Southern Hemisphere storms depicted in Fig. 9a, radius from the storm center in degrees of latitude vs pressure in hPa, for (a) temperature anomaly from the average at a distance of nine model grid points from the center, (b) relative humidity, and (c) tangential velocity. Contour interval is 1°C for (a), 10% for (b), and 2 m s^{-1} for (c).

we concentrate on the results for the areas around Australia. Figure 13 shows the composite structure of all the detected TCLVs shown in Fig. 9a for regions south of the equator. This structure may be compared to the observed composites of Frank (1977), which are shown in Fig. 14. Values are plotted as radial averages around the storm center. The temperature structure is shown in Fig. 13a; here, temperature anomalies at each level are calculated relative to mean temperatures at a radius of nine grid points (about 10.2° of latitude) from the center of each storm. Greatest temperature anomalies are seen in the upper troposphere near 400 hPa, slightly lower in the atmosphere than shown in the Frank composites, where maximum temperature anomalies usually occur closer to 300 hPa. This result may be related to the tropopause height in the DARLAM simulation (see Fig. 3). Both these factors may be related to the coarse vertical resolution of the model.

The relative humidity profile (Fig. 13b) is also reason-

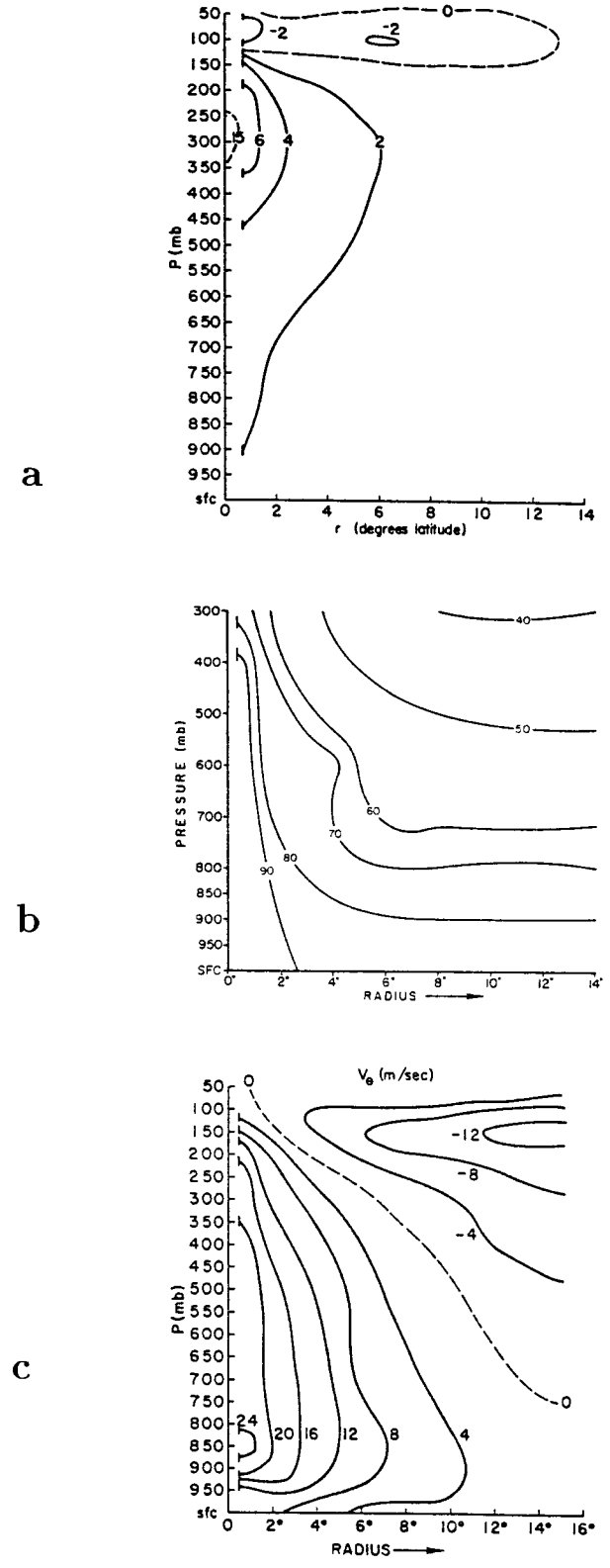

FIG. 14. The same variables as in Fig. 13 but from the Frank (1977) observed composites. Contour interval is 2°C for (a), 10% for (b), and 4 m s^{-1} for (c).

ably similar to observed, with maximum values in the lower troposphere close to the storm center. The vertical mixing of moist air does not appear to be as effective in the simulations as it is in reality, where relative humidities in excess of 90% are observed as high as 400 hPa. Finally, the structure of tangential wind velocity with height (Fig. 13c) has several similarities to reality: largest values are at low levels, and velocities mostly decrease upward and outward, becoming negative in the upper troposphere some distance away from the storm. One main difference between the simulated and observed tangential wind velocities is that the simulated values reach a maximum near a radius of 3° of latitude and decline closer to the storm center, whereas in reality the region of maximum winds associated with the eyewall is typically much closer to the storm center, about 10–100 km, as mentioned above. With maximum tangential wind speeds some 300 km from the storm center, the model is still not resolving the main structural features of tropical cyclones (i.e., the eye and eyewall). This difference in structure may be at least partly a result of the coarse horizontal resolution of the model. A similar structure was seen in simulations of B95, although they give similar vertical profiles only for a single storm, not a composite. The distance from the center of the storm to the region of maximum wind speed was also shown in their work to be a function of the horizontal resolution of the model, as we have shown in the previous section (see also Krishnamurti and Oosterhof 1989).

A measure of intensity that may enable a more resolution-independent comparison between the simulated vortices and observed tropical cyclones is angular momentum. Since angular momentum is a function of radius from the center of the storm, it may therefore be a more general measure of intensity when comparing the weaker, larger simulated storms to the stronger, smaller observed ones. Figure 15a shows the angular momentum for the DARLAM composite, while Fig. 15b shows the observed angular momentum digitized and calculated from the Frank (1977) composite of tangential wind speed shown in Fig. 14c. While the angular momentum structure of the model composite is similar to observed, some differences do occur: the simulated storms generally have larger angular momentum in the lower atmosphere, except for a region closer to the storm center, where the observed values are higher. But given the differences in the methodologies by which they were compiled, the two composites are quite similar.

The composite structure of the LAM vortices can also be compared to those generated by the GCM in the Southern Hemisphere. It might be expected that the GCM, being of much lower resolution than the LAM, would produce a much less realistic simulation of TCLVs. There are a couple of considerations that need to be mentioned first, however. Because the Gaussian grid of the GCM is much coarser than that of the LAM, the detection routine was required to search for wind maxima around the detected GCM vortex centers over a much wider area than that used for the LAM. Wind

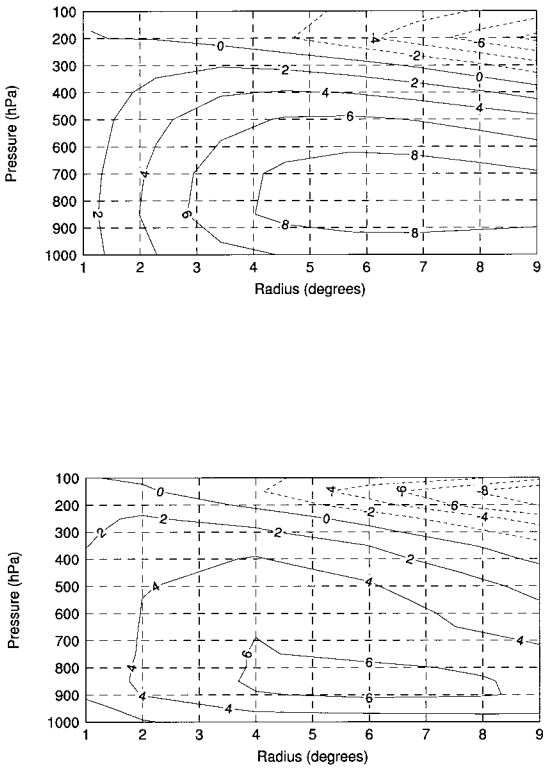

FIG. 15. Angular momentum calculated from tangential wind composites for (a) DARLAM and (b) the Frank (1977) observations. Contour interval is 2×10^6 m^2 s^{-1}.

maxima in the GCM vortices tended to occur about 5°–10° of latitude away from the detected centers, versus 2°–3° (typically) for the LAM. The OCS criterion is not relevant to the GCM vortices, as the OCS region is subgrid scale at the resolution of the GCM. The GCM vortices were thus detected using a threshold maximum gridpoint wind speed criterion, in addition to the other criteria previously described. Examination of several GCM vortices showed that they were much less clearly defined than the LAM vortices and were more likely to be asymmetrical. The composite tangential wind speed for all detected vortices in the GCM with a threshold maximum 10-m wind speed of at least 10 m s^{-1} is shown in Fig. 16. The region of maximum tangential wind speed is farther out from the center than in the LAM results and substantially weaker. The numbers of GCM-generated vortices stronger than this threshold were fewer than those generated by the LAM at the same threshold: in the GCM, 42 vortex days were found, versus more than 100 for the LAM. The GCM greatly underestimates observed radial average intensities, much more so than the LAM (see below). The LAM also generates more realistic results for temperature anomaly and relativity humidity profiles (Figs. 16a,b).

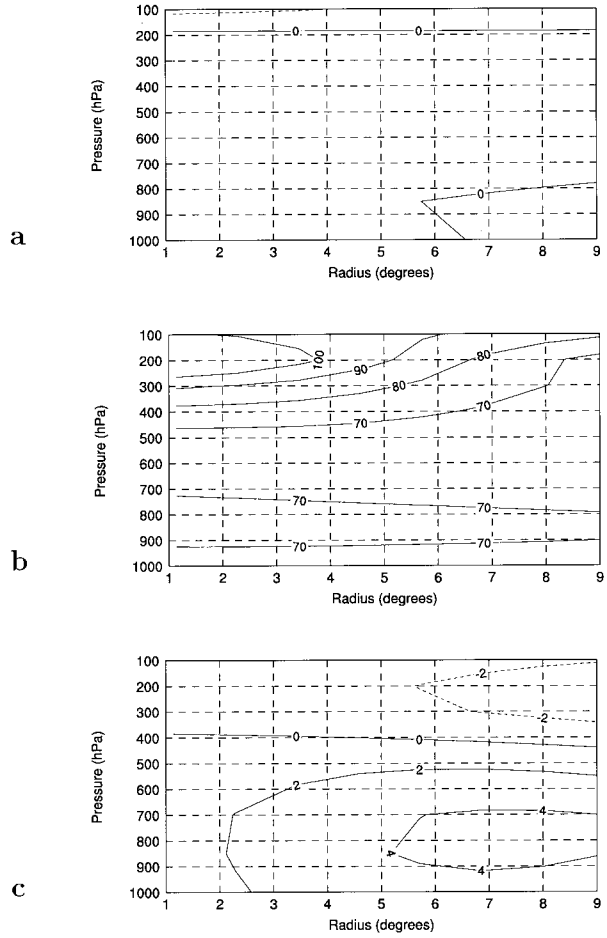

FIG. 16. Composite TCLV structure for all Southern Hemisphere storms detected in the GCM, radius from the storm center in degrees of latitude vs pressure in hPa, for (a) temperature anomaly from the average at a distance of nine model grid points from the center, (b) relative humidity, and (c) tangential velocity. Contour interval is 1°C for (a), 10% for (b), and 2 m s^{-1} for (c).

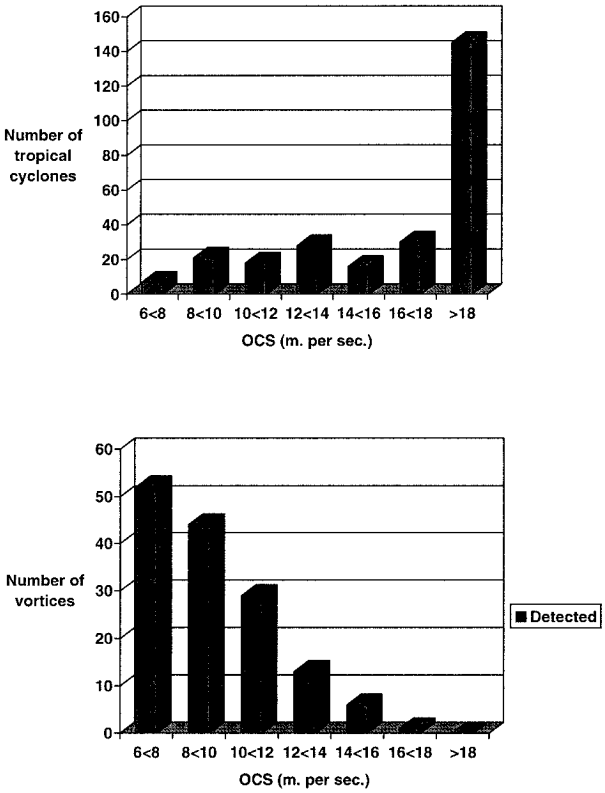

FIG. 17. Histograms of OCS for (top) tropical cyclone observations of Weatherford and Gray (1988b) and (bottom) TCLVs simulated by DARLAM.

f. TCLV intensities

Here we examine snapshots of storm characteristics on individual days rather than a mean or maximum intensity taken over several days. Figure 17a shows a histogram of OCS taken from the observations shown in Fig. 1 of Weatherford and Gray (1988b); here we select tropical cyclones with an OCS of greater than 6 m s^{-1}. We can compare the same results for the simulated Southern Hemisphere TCLVs (Fig. 17b). In the DARLAM simulation, there are no TCLVs with an OCS greater than 18 m s^{-1}, whereas in the Weatherford and Gray observations, roughly half of the observed cyclones of tropical storm strength or greater had an OCS larger than this figure. Despite the fact that there are more intense storms observed in the North Pacific than in the regions around Australia, this result strongly suggests that the TCLVs in the 125-km simulation are in general weaker than observed tropical cyclones, even when a large-scale variable such as OCS is used for comparison instead of maximum wind speeds. Intensities are generally greater in the 30-km simulation, however. Additionally, the TCLV distribution of Fig. 17b appears much more skewed toward weak storms than the observed tropical cyclone distribution. The histogram comparison may be less valuable for weak storms, as the threshold for the detection of tropical cyclones of less than tropical storm strength in the observations may be somewhat different from that used in the DARLAM simulation. Even though we have assumed that TCLVs must have a definite cyclonic vorticity and that they must have a vertical temperature and wind structure characteristic of observed tropical cyclones, it is possible that at least some of the relative abundance of weak TCLVs simulated by DARLAM may be a result of a mismatch between the DARLAM detection criteria and those used operationally for collecting the data analyzed by Weatherford and Gray (1988a,b). Nevertheless, this result suggests that the OCS distributions of the simulated TCLVs and observed tropical cyclones are substantially different.

Figure 18 shows the relationship between OCS and the maximum wind speed of the Southern Hemisphere TCLVs. There appears to be a closer relationship between the two variables for the TCLVs than occurs in reality, in particular

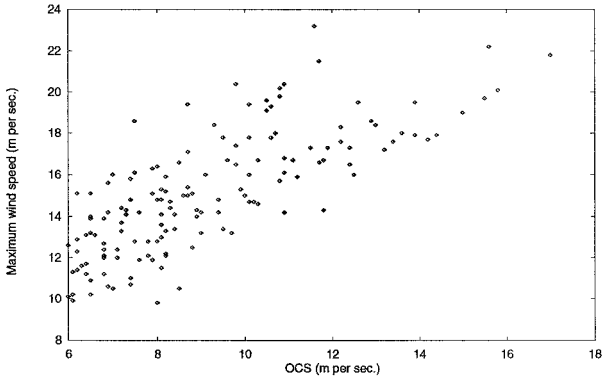

FIG. 18. Scatterp1ot of OCS versus maximum winds for all TCLVs with an OCS of at least 6 m s^{-1}.

for intense TCLVs. In real tropical cyclones, there is little relationship between OCS and maximum wind speed for intense storms (Weatherford and Gray 1988b). The closer relationship simulated in DARLAM is again probably a function of the limited resolution of the model, since in DARLAM maximum wind speeds typically occur in the same region as that used to calculate the OCS, whereas maximum wind speeds in observed tropical cyclones are usually closer to the center of the storm than the OCS region. There are 39 storm days with a maximum 10-m wind speed of at least 17 m s^{-1} (the tropical storm threshold), compared to 49 storm days with an OCS of at least 10 m s^{-1}, which implies that if TCLVs were defined on the basis of the observed maximum 10-m wind speed threshold for a tropical storm instead of the OCS threshold, fewer would be detected. There is also a relationship in the simulated TCLVs between the OCS and the strength of the warm core as measured by the TTOT (not shown). This correlation is also best for more intense storms, typically those with an OCS greater than about 10 m $s^{-1.}$

4. Discussion

Any comparison between observed tropical cyclones and the TCLVs generated by the LAM must recognize the structural differences in the wind field between the simulated TCLVs and observed tropical cyclones, where the simulated vortices have wind maxima in the OCS region, and the region of observed maximum wind is subgrid scale in the model. There may be several possible reasons why the LAM underestimates the typical observed OCS distribution of tropical cyclones. The analysis of section 3d, using the components of Gray's SGP as diagnostic parameters, showed that the generation of storms in the LAM was strongly influenced by the low-level mean pattern of vorticity. Given that the mean vorticity is generally higher than observed close to Australia in the LAM simulation, however, this is probably not a factor in the generation of numbers of storms stronger than a specified threshold. In the simulations of Walsh and McGregor (1995), the LAM incorporated some horizontal diffusion. When the same simulation was performed without horizontal diffusion, the OCS of the TCLVs increased by some 50%, although the typical OCS was still less than observed. The choice of convective parameterization in the LAM may also play a role. The version of the model employed here used a modification of the Kuo (1974) parameterization for convection. It has been shown that there is some sensitivity of simulated tropical cyclone structure and intensity to the choice of convective parameterization (e.g., Baik et al. 1992; Kain and Fritsch 1995; Kasahara et al. 1996). It may be that in the same simulation with a different choice of parameterization, there may be different numbers and intensities of TCLVs.

Horizontal resolution is no doubt crucial, although B95 found that their spectral model simulation gave much higher maximum wind speeds, with results closer to reality. As shown in the multiply nested 30-km simulation, both the maximum wind speeds and the OCS of the generated vortices generally increase substantially with increasing resolution. Since the OCS distribution of the vortices simulated at 125-km resolution shows that they are mostly too weak, a higher-resolution simulation that increases intensities is likely to be an improvement. Because of the economy of the multiply nested technique in terms of computer resources, it may be used to simulate a number of storms at high resolution and thus obtain the same kind of comparison to climatology examined in this study for the 125-km simulations.

The analysis has shown that there is some relationship between the SGP and the pattern and numbers of cyclones generated internally in the LAM. Since the large-scale fields in the LAM usually resemble those in the forcing GCM, this suggests that the SGP may be used to diagnose in advance the likelihood that a particular GCM simulation could be used to drive a LAM and give a good climatology of TCLVs. Nevertheless, while the cyclogenesis characteristics of one TCLV were examined and found to be similar in some respects to observations, it has not been proven that cyclogenesis in the LAM is occurring in the same fashion as in reality. The present modeling system shows some potential for use in climate change predictions of numbers of TCLVs in regions where the large-scale climatology of the LAM is adequate. Further progress will depend upon improvements in both the GCM and the LAM.

5. Conclusions

The tropical climatology of a limited area model (LAM) is assessed, and the characteristics of tropical low pressure systems generated by the model (tropical cyclone–like vortices, TCLVs) are examined. The simulated TCLVs have some of the observed physical characteristics of tropical cyclones and are much more realistic than similar vortices generated by the GCM. Genesis occurs at realistic rates in several regions and largely in observed locations, and the tracks and typical life cycles of TCLVs are similar to observed, except in the North Pacific region, where the mean

climate of the GCM and the limited area model are less adequate. The composite structure of the TCLVs has many similarities to that observed for tropical cylones, including low-level wind maxima, positive midtropospheric temperature anomalies, and intense convection. Such features as an eye and an eyewall are of course not resolved by the model. Maximum winds tend to be located farther from the centers of the TCLVs than observed, which is likely a result of the coarse horizontal resolution of the model. When the distribution of large-scale low-level wind speeds in the TCLVs is compared to observations, it is found that TCLVs are considerably less intense on average than observed tropical cyclones. Thus the greatest potential for prediction using the model exists for genesis locations, numbers, and tracks. Little potential exists at this time for predictions regarding TCLV intensities.

We use the components of Gray's Seasonal Genesis Parameter (SGP) to diagnose the reasons for the LAM's simulated pattern of cyclogenesis. Model cyclogenesis is strongly influenced by mean low-level values of cyclonic vorticity, as observed. Relative humidity values provide an important threshold for model cyclogenesis. A comparison between the SGP field diagnosed from the mean climate and the internally generated cyclogenesis of the LAM suggests is made. Our analysis shows that although the SGP has some ability to predict model cyclogenesis, it is not a definitive measure. Although it is likely that if a longer model simulation was performed, the SGP would demonstrate more skill, the analysis suggests that a reformulation of the SGP in this context may be warranted.

Two of the main limitations of climate models are their low horizontal and vertical resolutions and their inadequate representation of moist convective processes. These constraints are particularly important when trying to simulate small, convectively driven systems like tropical cyclones. Nevertheless, the TCLVs simulated by DARLAM are similar in a number of respects to observed tropical cyclones and give us some encouragement that more realistic results (particularly with regard to intensities) can be obtained with higher resolution and better convective parameterizations. Using a multiply nested simulation at a horizontal resolution of 30 km, we show that the intensity of the generated TCLV is greater and, thereby, is likely to be more realistic.

One can envisage an ideal experiment in which a climate model of very high horizontal resolution (of the order of a few kilometers) and excellent physical parameterizations is used to assess changes in numbers, distributions, and intensities of tropical cyclones as a result of climate change. Nevertheless, a great deal of work remains before all three of these factors can be reliably simulated using such an approach.

Acknowledgments. We would like to thank Jack Katzfey and John McGregor for useful conversations and the use of DARLAM model output. We thank Frank Woodcock, Noel Davidson, and Bill Frank for discussions on some of the material in this paper. We particularly thank Barrie Pittock and John McBride, as well as two anonymous reviewers, for their detailed comments. We gratefully acknowledge the financial support of the governments of the Northern Territory, Western Australia, and Queensland, and of CSIRO. We thank ECMWF for supplying the global analyses used here.

APPENDIX

Gray's Seasonal Genesis Parameter

The SGP is defined as

SGP = (vorticity parameter)(Coriolis parameter)
× (vertical shear parameter)
× (ocean energy parameter)
× (moist stability parameter)
× (humidity parameter),

where

vorticity parameter
≡ $|\zeta_r| + 5$, where ζ_r is relative vorticity in units of 10^{-6} s^{-1};

Coriolis parameter
≡ $|f|$;

vertical shear parameter
≡ $1/(S_z + 3)$, where $S_z = |\partial \mathbf{V}/\partial p|$ is taken between 950 and 200 hPa and is in units of m s^{-1} (750 hPa)$^{-1}$;

ocean energy parameter
≡ $\int \rho_w c_w (T - 26)\, dz$, where T is the sea temperature, ρ_w is the water density, and c_w is the water heat capacity; the integral is taken from the surface to 60 m or to where $T = 26$°C; and units are 0.42 J m^{-2};

moist stability parameter
≡ $\partial\theta_e/\partial p + 5$, where $\partial\theta_e/\partial p$ is taken between the surface and 500 hPa and has the units K/(500 hPa);

humidity parameter
≡ (RH − 40)/30, where RH is the mean relative humidity between 500 and 700 hPa but defined as zero for RH ≤ 40, and 1 for RH ≥ 70.

In the analysis presented here, climatological sea surface temperatures were used in both the LAM and the forcing GCM simulations, so this parameter is not included in the analysis of differences between these simulations or between them and observations.

REFERENCES

Anthes, R. A., 1982: *Tropical Cyclones: Their Evolution, Structure and Effects. Meteor. Monogr.,* No. 41, Amer. Meteor. Soc., 208 pp.

Atkinson, G. D., and C. R. Holliday, 1977: Tropical cyclone minimum sea level pressure maximum sustained wind relationship for the western North Pacific. *Mon. Wea. Rev.,* **105,** 421–427.

Baik, J.-J., M. DeMaria, and S. Raman, 1992: A comparison of deep cumulus parameterization schemes in an axi-symmetric tropical cyclone model. *Physical Processes in Atmospheric Models,* D. R. Sikka and S. S. Singh, Eds., Wiley and Sons, 149–156.

Bengtsson, L., M. Botzet, and M. Esch, 1995: Hurricane-type vortices in a general circulation model. *Tellus,* **47A,** 175–196.

Boer, G. J., and Coauthors, 1992: Some results from an intercomparison of the climates simulated by 14 atmospheric general circulation models. *J. Geophys. Res.,* **97,** 12 771–12 786.

Broccoli, A. J., and S. Manabe, 1990: Can existing climate models be used to study anthropogenic changes in tropical cyclone climate? *Geophys. Res. Lett.,* **17,** 1917–1920.

Davidson, N. E., and A. Kumar, 1990: Numerical simulation of the development of AMEX Tropical Cyclone Irma. *Mon. Wea. Rev.,* **118,** 2001–2019.

——, G. J. Holland, J. L. McBride, and T. D. Keenan, 1990: On the formation of AMEX Tropical Cyclones Irma and Jason. *Mon. Wea. Rev.,* **118,** 1981–2000.

Elsberry, R. L., 1995: Tropical cyclone motion. Global perspectives on tropical cyclones, WMO/TD-No. 693, 289 pp. [Available from World Meteorological Organization, Case Postale 2300, CH-1211 Geneva 2, Switzerland.]

Emanuel, K. A., 1994: *Atmospheric Convection.* Oxford University Press, 580 pp.

Frank, W. M., 1977: The structure and energetics of the tropical cyclone. I. Storm structure. *Mon. Wea. Rev.,* **105,** 1119–1135.

——, 1987: Tropical cyclone formation. *A Global View of Tropical Cyclones,* Office of Naval Research, 53–90.

Giorgi, F., G. T. Bates, and S. J. Nieman, 1993: The multiyear surface climatology of a regional atmospheric model over the western United States. *J. Climate,* **6,** 75–95.

——, C. S. Brodeur, and G. T. Bates, 1994: Regional climate change scenarios over the United States produced with a nested regional climate model. *J. Climate,* **7,** 375–399.

Gordon, H. B., 1981: A flux formulation of the spectral atmospheric equations suitable for use in long-term climate modeling. *Mon. Wea. Rev.,* **109,** 56–64.

Gray, W. M., 1975: Tropical cyclone genesis. Dept. of Atmospheric Sciences Paper 234, Colorado State University, Ft. Collins, CO, 121 pp. [Available from Department of Atmospheric Science, Colorado State University, Fort Collins, CO 80523.]

——, 1979: Hurricanes: Their formation, structure and likely role in the tropical circulation. *Meteorology over the Tropical Oceans,* James Glaisher House, 155–218.

Haarsma, R. J., J. F. B. Mitchell, and C. A. Senior, 1993: Tropical disturbances in a GCM. *Climate Dyn.,* **8,** 247–527.

Hirakuchi, H., and F. Giorgi, 1995: Multi-year present day and $2\times CO_2$ simulations of monsoon-dominated climate over eastern Asia and Japan with a regional climate model nested in a general circulation model. *J. Geophys. Res.,* **100,** 21 105–21 126.

Holland, G. J., 1993: Ready reckoner. Global guide to tropical cyclone forecasting. WMO/TC-No. 560, Rep. TCP-31, World Meteorological Organization. [Available from World Meteorological Organization, Case Postale 2300, CH-1211 Geneva 2, Switzerland.]

Hurrell, J. W., 1995: Comparison of NCAR Community Climate Model (CCM) climates. *Climate Dyn.,* **11,** 25–50.

Kain, J. S., and J. M. Fritsch, 1995: Interactions between convective and stratiform precipitation regimes in meso β-scale simulations of a tropical cyclone. *Proc. 21st Conf. on Hurricanes and Tropical Meteorology,* Miami, FL, Amer. Meteor. Soc, 419–421.

Kasahara, A., J.-I. Tsutsui, and H. Hirakuchi, 1996: Inversion methods of three cumulus parameterizations for diabatic initialization of a tropical cyclone model. *Mon. Wea. Rev.,* **124,** 2304–2321.

Krishnamurti, T. N., and D. Oosterhof, 1989: Prediction of the life cycle of a supertyphoon with a high-resolution global model. *Bull. Amer. Meteor. Soc.,* **70,** 1218–1230.

——, H. S. Bedi, D. Oosterhof, and V. Hardiker, 1994: The formation of Hurricane Frederic of 1979. *Mon. Wea. Rev.,* **122,** 1050–1074.

Kuo, H. L., 1974: Further studies of the parameterization of the influence of cumulus convection on large-scale flow. *J. Atmos. Sci.,* **31,** 1232–1240.

Legates, D. R., and C. J. Willmott, 1990: Mean seasonal and spatial variability in gauge corrected global precipitation. *Int. J. Climatol.,* **10,** 111–127.

Liu, Y., F. Giorgi, and W. M. Washington, 1994: Simualtion of summer monsoon climate over east Asia with an NCAR Regional Climate Model. *Mon. Wea. Rev.,* **122,** 2331–2348.

McBride, J. L., 1995: Tropical cyclone formation. Global perspectives on tropical cyclones, WMO/TD-No. 693, 289 pp. [Available from World Meteorological Organization, Case Postale 2300, CH-1211 Geneva 2, Switzerland.]

——, and R. Zehr, 1981: Observational analysis of tropical cyclone formation. Part II: Comparison of non-developing versus developing systems. *J. Atmos. Sci.,* **38,** 1132–1151.

McGregor, J. L., 1987: Accuracy and initialization of a two-time-level split semi-Lagrangian model. *J. Meteor. Soc. Japan* (Special Volume), 233–246.

——, and K. Walsh, 1993: Nested simulations of perpetual January climate over the Australian region. *J. Geophys. Res.,* **98,** 22 283–23 290.

——, and ——, 1994: Climate change simulations of Tasmanian precipitation using multiple nesting. *J. Geophys. Res.,* **99,** 20 889–20 905.

——, H. B. Gordon, I. G. Watterson, M. R. Dix, and L. D. Rotstayn, 1993: The CSIRO 9-level atmospheric general circulation model. CSIRO Aust. Div. Atmos. Res. Tech. Paper 26, 89 pp. [Available from CSIRO Division of Atmospheric Research, PMB 1, Aspendale, Victoria 3195, Australia.]

NOAA, 1994: *World-wide Consolidated Tropical Cyclone Dataset TD 9636, 1871–1989.* NOAA, CD-ROM. [Available from WeatherDisc Associates, Inc., 4584 NE 89th, Seattle, WA 98115.]

Ruprecht, E., and W. M. Gray, 1976: Analysis of satellite-observed tropical cloud clusters. Part I: Wind and dynamic fields. *Tellus,* **28,** 391–413.

Trenberth, K. E., 1992: Global analyses from ECMWF and atlas of 1000 to 10 mb circulation statistics. NCAR Tech. Note NCAR/TN-373+STR, 191 pp. [Available from NCAR, P.O. Box 3000, Boulder, CO 80307-3000.]

——, and C. J. Guillemot, 1995: Evaluation of the global atmospheric moisture budget as seen from analyses. *J. Climate,* **8,** 2255–2272.

Tsutsui, J.-I., and A. Kasahara, 1996: Simulated tropical cyclones using the National Center for Atmospheric Research community climate model. *J. Geophys. Res.,* **101,** 15 013–15 032.

Tuleya, R. E., 1988: A numerical study of the genesis of tropical storms observed during the FGGE year. *Mon. Wea. Rev.,* **116,** 1188–1208.

Walsh, K., 1997: Objective detection of tropical cyclones in high-resolution analyses. *Mon. Wea. Rev.,* **125,** 1767–1779.

——, and J. L. McGregor, 1995: January and July climate simulations over the Australian region using a limited-area model. *J. Climate,* **8,** 2387–2403.

Watterson, I. G., M. R. Dix, H. B. Gordon, and J. L. McGregor, 1995a: The CSIRO nine-level atmospheric general circulation model and its equilibrium present and doubled CO_2 climates. *Aust. Meteor. Mag.,* **44,** 111–127.

——, J. L. Evans, and B. F. Ryan, 1995b: Seasonal and interannual variability of tropical cyclogenesis: Diagnostics from large-scale fields. *J. Climate,* **8,** 3052–3066.

Weatherford, C. L., and W. M. Gray, 1988a: Typhoon structure as revealed by aircraft reconnaisance. Part I: Data analysis and climatology. *Mon. Wea. Rev.,* **116,** 1032–1043.

——, and ——, 1988b: Typhoon structure as revealed by aircraft reconnaisance. Part II: Structural variability. *Mon. Wea. Rev.,* **116,** 1044–1056.

Wu, G., and N.-C. Lau, 1992: A GCM simulation of the relationship between tropical-storm formation and ENSO. *Mon. Wea. Rev.,* **120,** 958–977.